Discovery of Novel Small-Molecule Inhibitors of BRD4 Using Structure-Based Virtual Screening

Lewis R. Vidler,[†] Panagis Filippakopoulos,[‡,§] Oleg Fedorov,[‡,‖] Sarah Picaud,[‡] Sarah Martin,[‡,‖] Michael Tomsett,[†] Hannah Woodward,[†] Nathan Brown,[†] Stefan Knapp,*[,‡,‖] and Swen Hoelder*[,†]
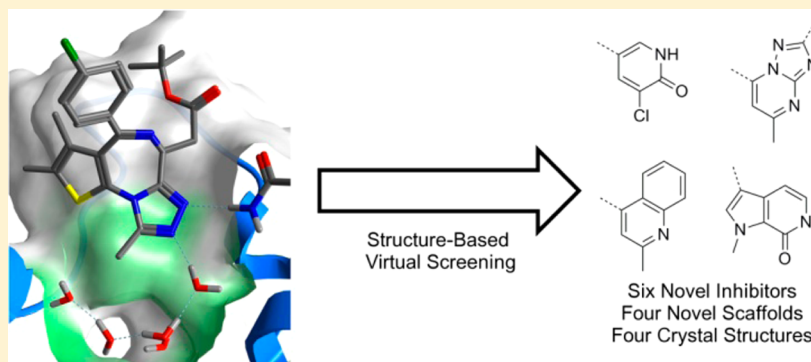
[†]Division of Cancer Therapeutics, Cancer Research UK Cancer Therapeutics Unit, The Institute of Cancer Research, 15 Cotswold Road, Sutton, Surrey SM2 5NG, United Kingdom

[‡]Nuffield Department of Clinical Medicine, Structural Genomics Consortium, Oxford University, Old Road Campus Research Building, Headington, Oxford OX3 7DQ, United Kingdom

[§]Ludwig Institute for Cancer Research, Old Road Campus Research Building, Headington, Oxford OX3 7DQ, United Kingdom

[‖]Nuffield Department of Clinical Medicine, Target Discovery Institute, Oxford University, NDM Research Building, Oxford OX3 7FZ, United Kingdom

S *Supporting Information*

Structure-Based Virtual Screening

Six Novel Inhibitors
Four Novel Scaffolds
Four Crystal Structures

ABSTRACT: Bromodomains (BRDs) are epigenetic readers that recognize acetylated-lysine (KAc) on proteins and are implicated in a number of diseases. We describe a virtual screening approach to identify BRD inhibitors. Key elements of this approach are the extensive design and use of substructure queries to compile a set of commercially available compounds featuring novel putative KAc mimetics and docking this set for final compound selection. We describe the validation of this approach by applying it to the first BRD of BRD4. The selection and testing of 143 compounds lead to the discovery of six novel hits, including four unprecedented KAc mimetics. We solved the crystal structure of four hits, determined their binding mode, and improved their potency through synthesis and the purchase of derivatives. This work provides a validated virtual screening approach that is applicable to other BRDs and describes novel KAc mimetics that can be further explored to design more potent inhibitors.

INTRODUCTION

The bromodomain (BRD) family of proteins recognize acetylated-lysine (KAc) in proteins and represent a set of protein–protein interaction modules that are becoming increasingly explored in the field of drug discovery.[1] The BET family of BRDs is a subset of this larger bromodomain family and is made up of four members: BRD2, BRD3, BRD4, and BRDT in humans, with each containing two BRD modules that share high sequence similarity[2] and highly similar binding sites.[3]

The BET family shares the same conserved tertiary structure of bromodomain proteins,[4−6] with the KAc binding site being formed as a central cavity by an atypical left-handed four-helix bundle flanked by the ZA loop and the BC loop (Figure 1A). This binding site is primarily hydrophobic, with key polar interactions being formed between the acetyl carbonyl of KAc and a family-conserved asparagine residue as well as a structurally conserved water molecule. Mimicking the interaction of this acetyl group has been the basis for generating small-molecule inhibitors of the readout function of the bromodomain proteins (Figure 1B), which was exemplified by the discovery of (+)-JQ1 (Figure 1C). Outside of the highly enclosed base of the pocket, inhibitors of the BET family have shown that occupying the adjacent regions, known as the hydrophobic shelf (occupied by phenyl in Figure 1C) and ZA channel (occupied by thiophene in Figure 1C), leads to
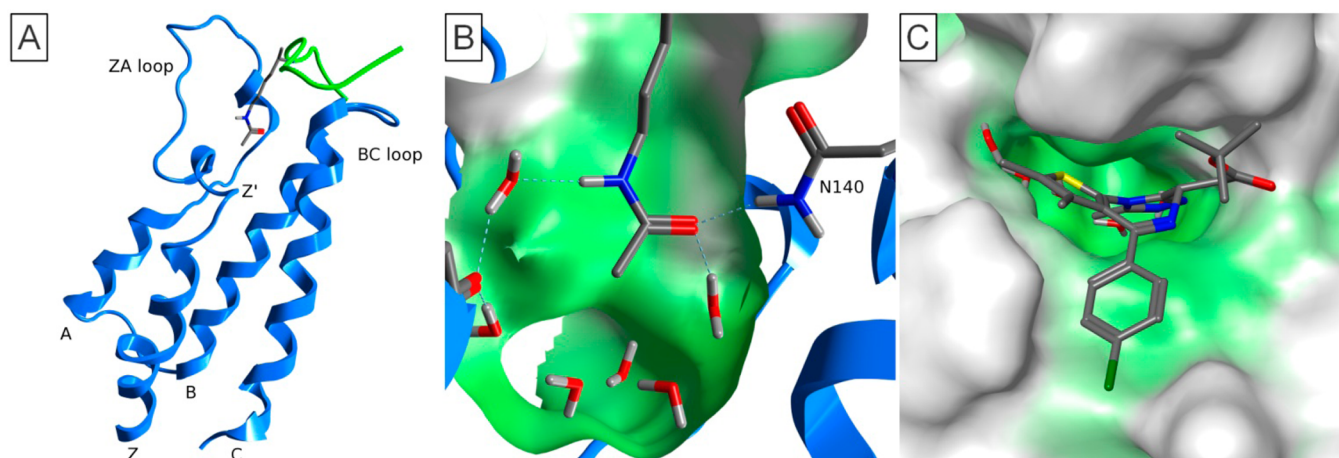
Figure 1. (A) Structure of first bromodomain of BRD4 bound to an acetylated peptide (PDB ID: 3UVW). (B) Interaction of KAc with BRD4 (PDB ID: 3UVW). (C) (+)-JQ1 bound to BRD4 with a chlorophenyl ring occupying the hydrophobic shelf and thiophene occupying the ZA channel (PDB ID: 3MXF). Surface colors were generated using the pocket colors in MOE. Green represents an enclosed surface, and white, exposed.
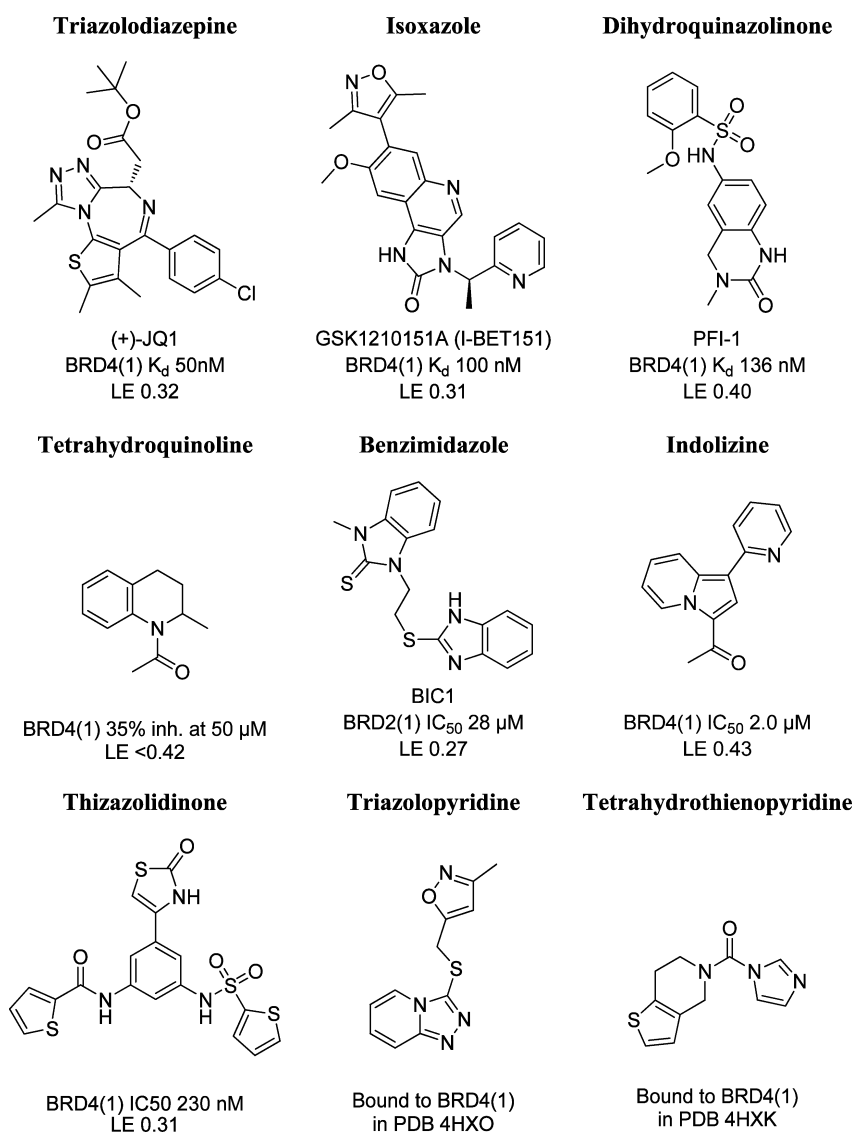

Figure 2. Structure, activity, and LE of published BET-family inhibitors classified by KAc mimetic.

nanomolar potency and a high degree of selectivity toward other bromodomains (Figures 1C and 2).[7−12]

The inhibition of the BET family of bromodomains has been proposed as a therapeutic strategy in multiple disease areas

including cancer, inflammation, and obesity.[1,13] Here, we have focused on BRD4, which was identified as a therapeutic target in AML,[14,15] other cancers,[16−18] and inflammatory disease,[12] as a representative member of the BET subfamily. A number of small-molecule inhibitors of BET family members have now been published.[19] A key feature of these inhibitors is a KAc mimetic that anchors the molecule into the BRD binding site via hydrogen bonds and hydrophobic interactions, which is critical for potent binding. A limited number of chemotypes that possess these features had been published when this work started and has been increasing (Figure 2). These include triazolodiazepine (e.g., (+)-JQ1),[7,8,12,20] isoxazole (e.g., GSK1210151A),[9,10,21−25] dihydroquinazolinone (e.g., PFI-1),[11,26,27] tetrahydroquinoline,[26] benzimidazole (e.g., BIC1),[28] indolizine,[26] thiazolidinone,[29] triazolopyridine,[29] and tetrahydrothienopyridine[29] scaffolds.

Upon starting this work, only the triazolodiazepine, dihydroquinazolinone, and benzimidazole KAc mimetics had been disclosed. To offer more possibilities for drug-design efforts against BRD4 and other bromodomains, we sought to identify novel chemotypes that can act as KAc mimetics. Different chemotypes binding to the same protein often show different physicochemical properties, distinct biological profiles, and offer additional opportunities for intellectual property generation.

Here, we describe a virtual screening approach that focuses on KAc mimetics and identifies novel scaffolds that fit this profile. Furthermore, we designed the virtual screen in a fashion largely independent of the bromodomain targeted, and we present the validation of the approach against BRD4.

The enclosed KAc binding site of bromodomains imposes strict geometric constraints on inhibitors, requiring excellent shape complementarity in this part of the pocket. To meet these constraints, we wanted to take advantage of the availability of BRD4 and other bromodomain crystal structures by utilizing molecular docking. However, the docking of several million commercially available compounds and in particular the processing of the results is still a time-consuming and labor-intense task. Frequently, methods of higher throughput, such as similarity- or pharmacophore-based searching, are used to select a smaller set of compounds that is then subjected to docking. Our approach to preselect a set of compounds for which docking can be managed recognizes the key role of the KAc mimetic in all known bromodomain inhibitors. We initially selected commercially available compounds that feature an KAc mimetic chemotype, that is, compounds that feature a moiety that has the potential to match the hydrogen-bond pattern and the steric constraints of the KAc binding site. Specifically, we created an extensive set of chemotpyes by exploring published data, intuitive design, and similarity searches. This set consisted of known chemotypes and, critically, also many chemical structures not yet described as bromodomain inhibitors. Next, we converted these chemotypes into substructures searches and retrieved commercially available compounds that feature these KAc mimetic substructures. This set of compounds was then subjected to docking against the first bromodomain of BRD4 (BRD4(1)). After an extensive filtering of the results and the purchasing and testing of selected compounds, we identified six inhibitors, including four unprecedented KAc mimetics. To validate our results further, we generated crystal structures of selected compounds bound to BRD4(1) and established early SAR around the novel chemotypes through synthesis and the purchase of derivatives.

Our work is relevant to scientists working on bromodomain inhibitors because it addresses three goals: first, through the focus on KAc mimetics, it efficiently preselects a subset of commercially available compounds and ensures that a large number of KAc mimetics are included in the docking step; second, through the docking step, it meets the tight geometric requirements of the KAc binding site; and third, this approach is applicable to other bromodomains for which crystal structures are available. Furthermore, we report an extensive compilation of novel chemotypes that can act as KAc mimetics and will thus be useful for other design approaches and scaffold hopping, and we report novel inhibitors of BRD4 that have the potential to be developed into significantly more potent compounds.

■ METHODS

Virtual Screening Approach. Our approach centered on identifying a series of chemotypes that had the potential to mimic KAc and fit the geometric constraints of the BRD4(1) binding pocket. These were then converted into substructure searches that were used to mine commercially available compounds for inhibitors of BRD4 using the eMolecules database.[30] We intended to generate these from two different branches. One branch we will refer to as the "Literature Substructures" branch, which was based on the KAc mimetic substructures extracted from published bromodomain inhibitors. These were also modified to generate structurally related substructures that maintained the key pharmacophore (e.g., 1,2,4-triazole to isoxazole). The other branch we will refer to as the "Similarity Searching" branch, which was based on pharmacophore, shape, and 2D fingerprint similarity searches derived from the published (+)-JQ1 and the crystal structure of it bound to BRD4(1) (PDB ID: 3MXF). The results of each of these branches was submitted to docking, and through a series of filters designed to reduce docking false positives, compounds were selected for purchase (Figure 3).

Literature Substructures Branch. We generated a library of bromodomain-focused substructures through the identification of the KAc mimetic substructure from published bromodomain inhibitors. To expand the number of substructures considered, we also included structurally related queries that maintained the key pharmacophore.
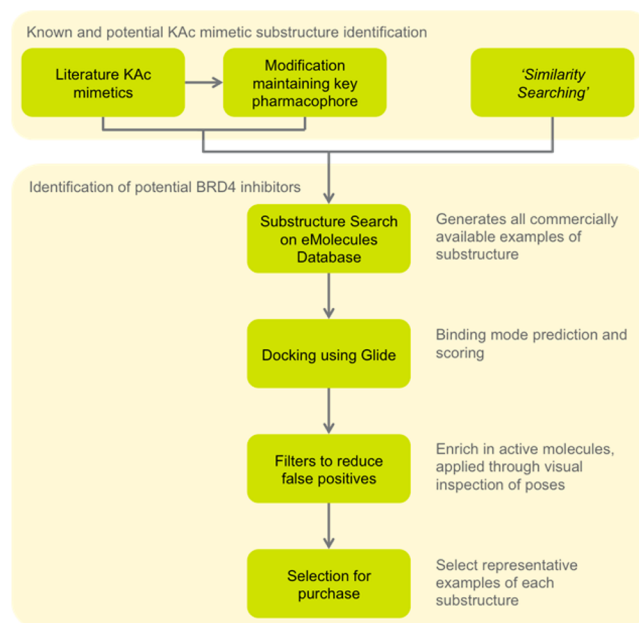

Figure 3. Flowchart summarizing the selection of compounds taken through to biochemical screening.
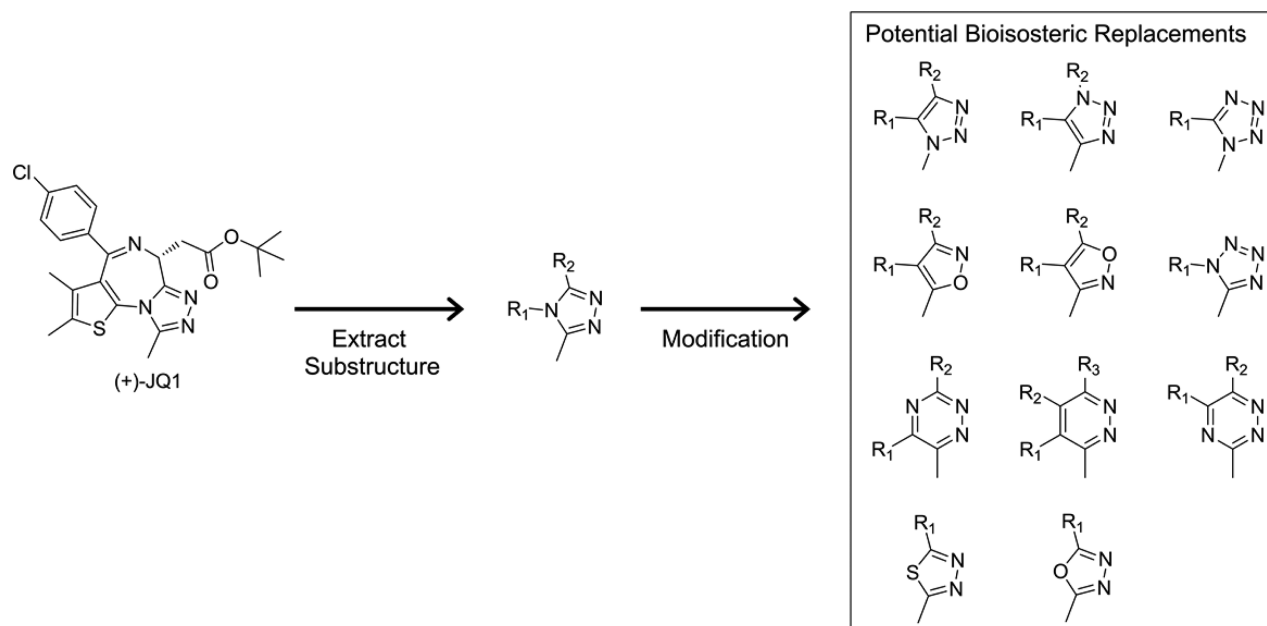
Figure 4. Example of the generation of substructures from (+)-JQ1 for the Literature Substructures approach.

An example of this approach starting from (+)-JQ1 is highlighted in Figure 4. The substructures carried forward to the rest of the approach are shown in the Supporting Information, Figure S1.

Similarity Searching Branch. With this branch, we were looking for novel KAc mimetics featuring chemotypes distinct from already known inhibitors. To identify such chemotypes, we used similarity searches (e.g., shape or pharmacophore) that allowed the identification of distinct chemotypes that nevertheless share the pharmacophoric features critical for binding of the probe compound (+)-JQ1. These similarity searches gave us a rich set of putative KAc mimetics from 2.4 million commercially available compounds. However, we reasoned that as a result of the tight geometric constraints of the BRD4 binding site many of these would not be able to bind, despite a high similarity, because even a simple change (e.g., from a methyl to an ethyl group) may lead to clashes within the KAc pocket. To enrich for compounds that fit the tight geometric constraint of the binding site, we thus performed a docking step and extracted KAc mimetics with sufficient shape complementarity. It is important to note that this docking step serves the purpose of creating a virtual library of KAc mimetics in conjunction with the similarity search and is distinct from the final docking step that will be described later and served the purpose of selecting compounds for purchase. The Similarity Searching branch is summarized in Figure 5.

Specifically, pharmacophore, shape, and 2D fingerprint searches were performed on 2.4 million commercially available compounds for the initial similarity search. Three pharmacophore searches were used, probing the base of the acetyl-lysine binding site, the hydrophobic shelf, and the ZA channel, using the structure of BRD4(1) as an excluded volume (PDB ID: 3MXF). The first search contained all of the features known to contribute to the potent binding of inhibitors: two acceptors within the acetyl-binding site at the base of the pocket as well as hydrophobic substituents in the ZA channel and the hydrophobic shelf positions. This placed fairly tight constraints on the molecules being screened against the probe, and as a result only a few molecules were able to match these criteria. To allow for more molecules to match and to focus on the KAc mimetic parts of the molecules, these constraints were relaxed by removing the requirement for the molecule to occupy the hydrophobic shelf. One further search was performed that required only one of the two acceptors within the acetyl binding site at the base of the pocket because examples of single-acceptor-atom KAc mimetics are known (e.g., dihydroquinazolinone derivatives). One shape-based and one 2D fingerprint similarity search were also applied to find molecules with a similar shape and similar
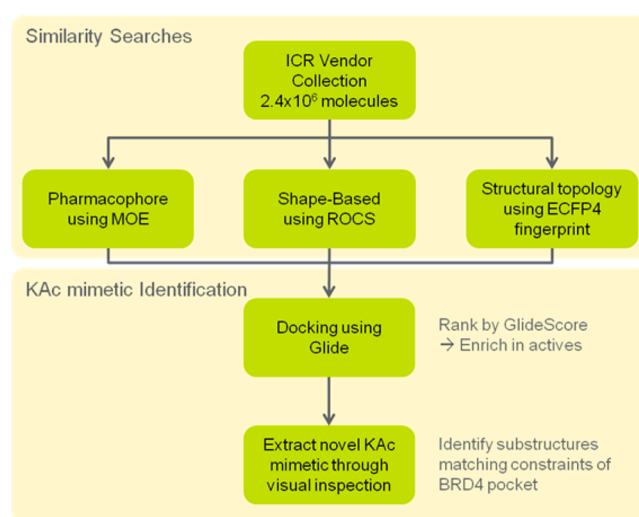

Figure 5. Flowchart summarizing the Similarity Searching branch of the virtual screen.

functional groups to the entire (+)-JQ1 molecule. One additional shape-based search was also applied to (+)-JQ1, with the chlorophenyl and tertiary-butyl ester removed to focus on the KAc part of the binding site. Each of these similarity searches was expected to identify different compounds and therefore maximize the chances of finding hits. Precise details of these similarity searches can be found in the Experimental Section.

Substructure Searches. A key step of our virtual screening approach was the use of an extensive set of substructures that we obtained from published data, intuitive design, and similarity searches, as already described. These substructures were consequently used to identify all commercially available examples of each of the substructures, employing substructure searches on the eMolecules database.[30] The results were then submitted to a second docking step and subsequent selection for purchase, as detailed below. This docking step was performed in the same manner as the one from the Similarity Searching branch, but it was necessary because of the different ligands present. It is important to note that this substructure search also ensured that all examples of a particular substructure of interest were identified and fed into the final docking step. This is in contrast to our
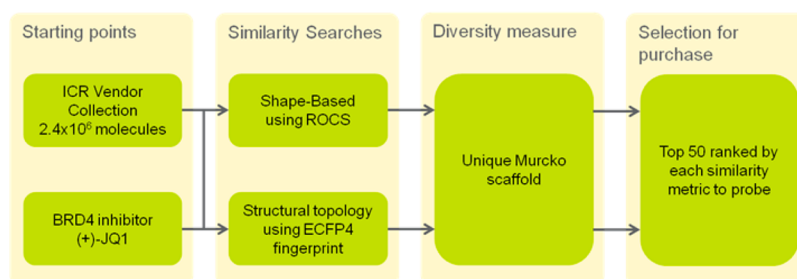
Figure 6. Flowchart summarizing the control experiment.

Table 1. Compounds Identified as Hits against BRD4(1) from the Virtual Screen

Compound Number	Structure	Source	Activity (μM IC$_{50}$ or % inhibition)	Follow up data gathered	UV Purity[a] (%)
1		Literature Substructures	4.7	IC$_{50}$ + crystal structure + active derivatives	>95
2		Literature Substructures	81	IC$_{50}$	>95
3		Similarity Searching	33% @ 125 μM	Crystal structure + active derivatives	>95[b]
4		Similarity Searching	32% @ 250 μM	Crystal structure + active derivatives	>95
5		Similarity Searching	31% @ 250 μM	Crystal structure + active derivative	>95
6		Similarity Searching	11% @ 100 μM	Active derivatives	>95

[a]See the Experimental Section for details. [b]Following HPLC purification of a commercial sample.

experience with similarity searches where a number of representatives of a particular chemotype are frequently missed, for example, because of different tautomers, protomers, or conformers of the starting library compounds.

Docking against BRD4(1), Reducing Docking False Positives, and Selecting Compounds for Purchase. The results of each of the substructure searches were subsequently docked against BRD4(1)

to predict the binding mode and to calculate a score, from which examples of each substructure can be selected for purchase. One of the limitations of using docking as a part of a virtual screen is that it generates false positives, reducing the enrichment of actives.[31,32] Docking comprises two key components: pose prediction and scoring.[33] Many of the false positives, however, involve the scoring of the molecules, with the pose generation considered to be sufficiently

accurate to be useful.[32,34] A recent report by Ferreira et al.[35] identified some of the underlying causes of false positives from docking. These include failure to penalize high-energy conformations of the molecules as well as the presence of heteroatoms that are not engaged in favorable interactions with the receptor.

Using this knowledge, we defined the following criteria that are necessary to be fulfilled by a molecule and its docking pose to be considered for purchase:

(1) No obvious high-energy conformations (using the CSD as validation) (see the Experimental Section for details).

(2) The majority of the heteroatoms form interactions with the receptor or are satisfied by internal hydrogen bonds, and key interactions defined by the hypothesis are formed.

(3) No clashes with the receptor or vacant sites unlikely to be filled by water molecules or protein movement.

(4) No reactive groups or groups known to interfere in biochemical assays.[36]

To implement these criteria, we manually inspected the docking poses as a pragmatic approach. This allowed for the defined criteria to be implemented quickly and each individual molecule to be considered on its own merit. At least 500 of the top ranked ligands from each docking run were inspected, and representative compounds from each scaffold that fulfilled these criteria were selected, resulting in a set of 150 compounds.

Control Experiment. Our approach is heavily based on docking and extensively takes advantage of human input for the final selection of compounds. To benchmark our approach, we sought a valid control experiment to compare our results to. Many retrospective analyses suggest that ligand-based methods frequently outperform the equivalent structure-based approaches when it comes to discriminating between active and inactive compounds;[37,38] therefore, we chose an experiment based on these approaches as a control. We based our selection on the same 2D fingerprint and shape-based similarity searches as the Similarity Searching part of our virtual screening approach starting from the entire (+)-JQ1 ligand and its bound conformation to BRD4(1), but in this experiment docking and subsequent visual inspection were not utilized.

To select compounds and to ensure that a minimum level of diversity was achieved, the top 50 compounds from each method, ranked by similarity to (+)-JQ1 with unique Murcko scaffolds,[39] were selected for purchase. One hundred compounds in total were selected using this approach in a fully automated way, and there was no overlap between the compounds selected by the control experiment and those from the virtual screen. The control experiment is summarized in Figure 6.

RESULTS AND DISCUSSION

Using our virtual screening protocol detailed above and including the compounds selected from the control experiment, 250 compounds were purchased and prepared as DMSO stock solutions. Ten of these compounds were insoluble in DMSO, and as such they were not carried forward to biochemical screening. The remaining 240 compounds were initially screened using the AlphaScreen assay format at a single concentration up to 250 μM,[40] depending on compound solubility. Six compounds exhibited an inhibition of BRD4(1), but only two of these compounds yielded an IC$_{50}$: **1** had an IC$_{50}$ of 4.7 μM, and **2** had an IC$_{50}$ of 80.9 μM. The IC$_{50}$ of the remaining compounds was higher than the solubility and as such could not be determined. Despite the modest activity of some of the hits, we next sought to cocrystallize all novel KAc mimetics that showed significant binding, and we obtained crystal structures of four compounds bound to BRD4(1). Finally, we investigated derivatives of five of these compounds through purchase and synthesis, yielding compounds that showed significantly improved activity. **2** was not followed up further because of publications appearing after the virtual

screen was performed detailing derivatives of this isoxazole scaffold.[9,10,21−25] The structures of these hits and the data gathered for each of the compounds are summarized in Table 1. The docking poses used to initially select these six compounds can be found in the Supporting Information, Figure S2.

Crystallography. Following the identification of six compounds as inhibitors of BRD4(1), crystal structures of four of the compounds in the KAc binding site were obtained (Figure 7). This allows the binding mode to be used to design more potent analogues and to compare the docking poses to
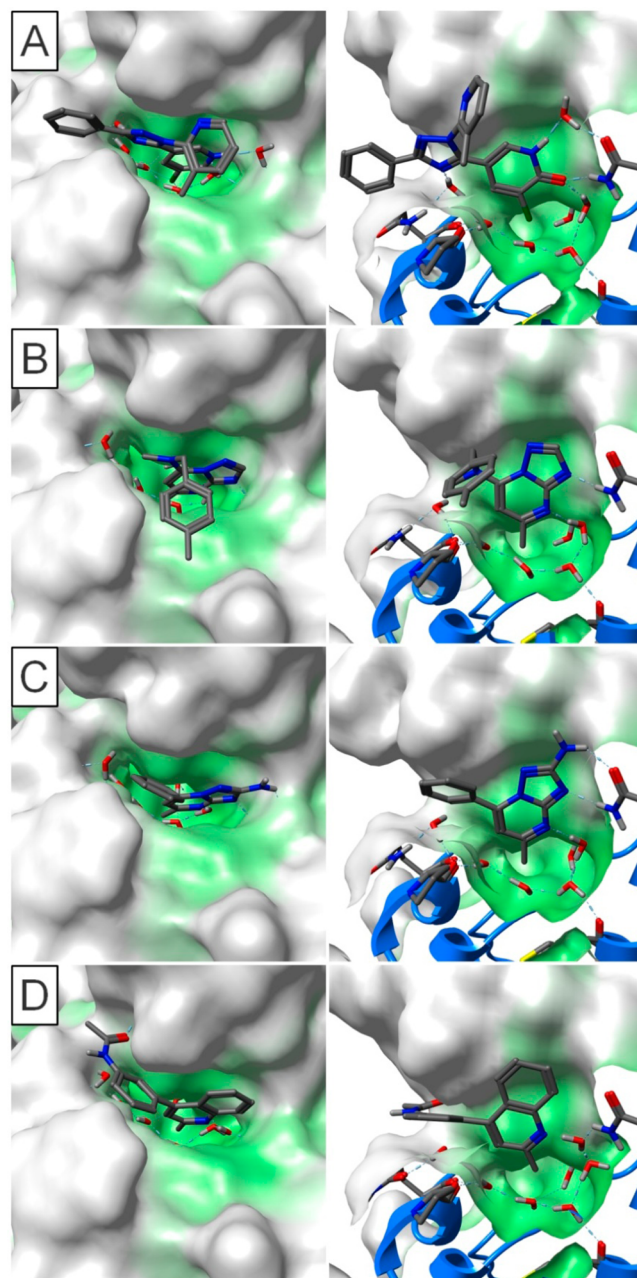

Figure 7. Crystal-structure binding modes of four of the identified inhibitors bound to BRD4(1). The left panel gives an overview of the binding mode. The right panel gives a through-protein view highlighting the binding mode of each KAc mimetic. Surface colors were generated using the pocket colors in MOE. Green represents an enclosed surface, and white, exposed. (A) Compound **1**, (B) compound **3**, (C) compound **4**, and (D) compound **5**.

the experimentally observed binding mode that the docking was trying to predict. Extremely high accuracy was attained for the docking of **3** and **4**, for which the docking poses were within experimental error of the crystal structure poses (rmsd ≤ 0.30 Å). In the case of these two compounds, the protein showed very limited movement from its conformation bound to (+)-JQ1 with an rmsd of 0.37 Å between the model used (PDB ID: 3MXF) and each of the triazolopyrimidine bound structures, which may have contributed to the success of the docking experiment. In the case of **1** and **5**, the docking predicted the experimentally observed pose of the ligand (rmsd < 2.0 Å) but with a few subtle differences. Some of these differences were the result of water molecules bridging interactions that the docking was unable to consider. Comparisons between the predicted and experimentally determined poses can be seen in Figure 8. Details of all of the crystallographic binding modes will be discussed in the context of each of the series below.
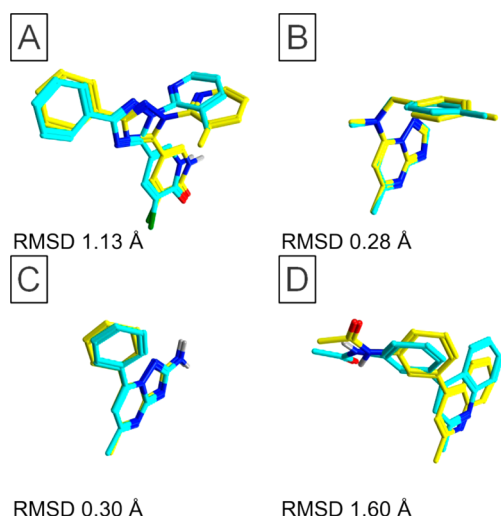

Figure 8. Overlay of the observed crystallographic pose (cyan carbons) with the docking pose in the model from PDB ID: 3MXF (yellow carbons) following alignment of the two proteins using MOE. (A) Compound **1**, (B) compound **3**, (C) compound **4**, and (D) compound **5**.

Compounds for which more information has been gathered will now be described.

Chloropyridones. The chloropyridone scaffold was selected using the Literature Substructures branch derived from the known dihydroquinazolinone inhibitors. The evolution of the initial dihydroquinazolinone substructure

involved the removal of the phenyl ring, and we hypothesized that the chloropyridone motif would be able to mimic the remaining dihydropyrimidone substructure (Figure 9). The carbonyl and NH donor were maintained through this modification, with the chlorine atom occupying the same location as the methyl group it replaced. A substructure search performed on the eMolecules database yielded 82 commercially available examples of this substructure. Following the docking and selection process detailed above, **1** and **7a** were selected for purchase.

1 was the most potent of the 240 compounds initially tested, with an IC$_{50}$ of 4.7 μM and associated LE of 0.28. Structurally related **7a**, also tested in the original batch of 240 compounds, was found to be inactive. The only other commercially available compounds containing the chloropyridone and triazole functionalities were **7b** and **7c**. These were subsequently purchased and tested (Table 2) and found to be significantly less active. A crystal structure of **1** bound to BRD4(1) was obtained with the carbonyl of the pyridone occupying a similar position to the carbonyl oxygen of the acetyl-group of KAc, forming the same interactions with the NH donor of the Asn140 side chain and conserved water molecule. The chlorine atom occupies the base of the pocket that the methyl group of KAc would usually occupy, and the NH donor of the pyridone forms a water-mediated hydrogen bond to the carbonyl of the conserved Asn140 side chain. This is the first example of a chlorine substituent occupying the base of the KAc binding pocket, which can potentially be incorporated into other templates, replacing the methyl group commonly used at this position. The remaining interactions of **1** involve the triazole that forms an interaction with one of the conserved water molecules and occupies the ZA-channel region of the pocket as well as hydrophobic interactions of the phenyl and pyridine rings (Figure 7A).

Triazolopyrimidines. **3** and **4** both contain the same triazolopyrimidine scaffold and were initially selected on the basis of the hypothesis that they mimic KAc. The observation that **3** and **4** show significant inhibition as well as, importantly, the cocrystal structures of these compounds with BRD4(1) validated this hypothesis and confirmed the triazolopyrimidine as a novel KAc mimetic. The triazolopyrimidine engages in the same interactions in both structures as the carbonyl of the acetyl group of KAc, albeit through two nitrogen atoms compared to each lone pair of the carbonyl (Figure 7). This strong complementarity is likely the reason for the accurate prediction of the docking experiment as well as for the minimal movement of the protein from the reference model (PDB ID: 3MXF).
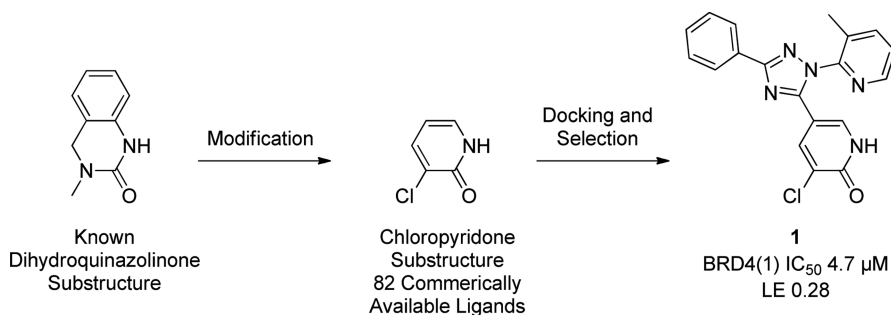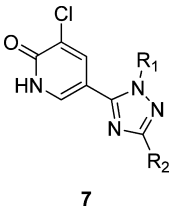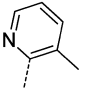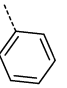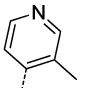

Figure 9. Evolution of **1** from known dihydroquinazolinone inhibitors.

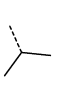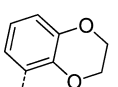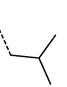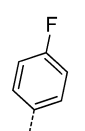**Table 2. Activity of Commercially Available Derivatives of the Chloropyridone Scaffold**

7

Compound number	R₁	R₂	IC₅₀[a] (μM)	LE	UV Purity[a] (%)
1			4.7	0.28	>95
7a			9% @ 100 μM	-	>95
7b			77	0.21	>95
7c		Me	17% @ 100 μM	-	>95

[a]See the Experimental Section for details.

A number of commercial derivatives of this scaffold were subsequently purchased (Supporting Information, Figure S3). Gratifyingly, **8b** demonstrated a substantially improved activity toward BRD4(1), with an IC₅₀ of 24 μM and associated LE of 0.33, demonstrating that this class of compounds can be further improved.

The comparison of the matched pair compounds **4** and **8a**, which only differ by the presence of an amino substitution at the triazolopyrimidine, suggested that introduction of the amino group into compounds **3** and **8b** may lead to an improvement of activity. The improvement in potency can be rationalized by the observation that the amino group forms an interaction with the conserved asparagine, as seen in the crystal structure of **4** with BRD4(1) (Figure 7C), and completes the acceptor−acceptor−donor motif that is observed for published inhibitors (e.g., dihydroquinazolinones) as well as some of the other inhibitors identified here (**2**, but also **1** and **6** if the carbonyl is considered as **2** acceptors). We thus prepared (Scheme 1) and tested compounds **8c−e**. **8c** showed indeed a

Scheme 1. Synthetic Route to 8e−g[a,b]

[a]R₁ corresponds to the functional group from Table 5. [b]Reagents and conditions: (a) POCl₃, reflux, 2 h; (b) R₁ amine, EtOH, reflux, 2 h.

significant improvement over **3** and **4**. Furthermore, the improved activity of **8c** over **4** is likely due to an interaction of the benzylamino group of **8c** with the hydrophobic shelf, as observed from the crystal structures of **3** bound to BRD4(1). This interaction is known to provide improvements in potency in other series of BET-family inhibitors, including (+)-JQ1, and is not found in the complex of **4** with BRD4(1). Compound **8d** shared comparable activity to **8c**, showing that the methylation of the benzylic amine is not required for activity. Finally, introduction of an amino group into **8b** to yield **8e** maintained the activity but in this case did not lead to an improvement in potency. However, compounds **8b−e** demonstrate that there is scope for further improvement of the initial hits **3** and **4** and that a reasonable LE (∼0.3) can be achieved.
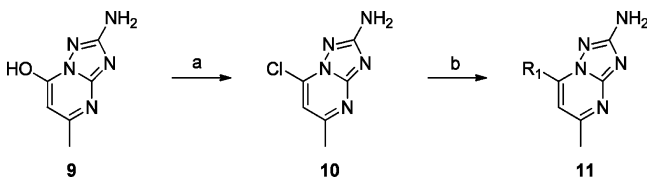
Quinolines. **5** demonstrated inhibition of BRD4(1), but its IC₅₀ was lower than its solubility and could not be determined; however, the crystal structure bound to BRD4(1) revealed two interesting features. First, the acetyl group was not acting as the KAc mimetic but formed an interaction with the backbone NH donor of Asp88, an interaction that has not been observed in any published bromodomain crystal structure to date (Figure 10). Although the crystallographic orientation of the molecule was predicted by the docking pose, this particular interaction with the backbone NH donor of Asp88 was not, suggesting another way in which potency and potentially selectivity can be achieved from the BRD4(1) binding site.

The second interesting feature of this binding mode is that the quinoline nitrogen does not appear to be forming a direct interaction with the protein. From the crystal structure, electron density could be observed in close proximity to the quinoline nitrogen (Figure 11), suggesting an interaction through a bridging water molecule. Interestingly, the distance between the oxygen of the water molecule and the ligand appeared to be very short (2.14 Å), and we speculated that the active ingredient of this compound was in fact the quinoline N-oxide; however, mass spectrometry did not detect the N-oxide. We nevertheless decided to synthesize the N-oxide **14a**, and **5** was resynthesized along with it (Scheme 2), and both compounds were tested for BRD4(1) inhibition.

The resynthesized batch of **5** demonstrated activity similar to the original sample, however, the pure N-oxide generated a significantly improved IC₅₀ of 42 μM (Table 4). This is a good example of a single-atom change in a ligand resulting in the displacement of a single water molecule and achieving an increase in activity.
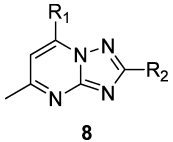
Pyrrolopyridones and Pyrrolopyrimidones. Although pyrrolopyridone **6** demonstrated the lowest activity of the compounds initially identified as hits, it also contained the fewest heavy atoms, suggesting decent ligand efficiency despite its modest activity. In addition, it represented another example of a novel KAc mimetic, and we sought to demonstrate that somewhat larger derivatives show improved inhibition. Although few pyrrolopyridones were commercially available, a number of related pyrrolopyrimidones could be sourced. Gratifyingly, the phenyl substituted compounds **15a** and **15b** showed substantially improved activities, with an LE above 0.3 (Table 5). These compounds represent attractive starting points for further development. This improvement in potency is consistent with the phenyl ring occupying the ZA channel, as would be expected from the docking pose of **6** (Supporting Information, Figure S2).

Comparison between the Branches of Our Virtual Screen. Within our virtual screening approach, two branches
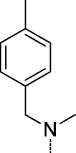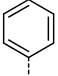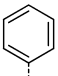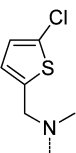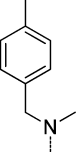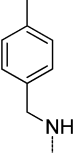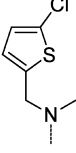
Table 3. SAR around the Triazolopyrimidine Scaffold

8

Compound number	R$_1$	R$_2$	IC$_{50}$^{a} (μM)	LE	UV Purity^a (%)
3		H	33% @ 125 μM	-	>95
4		NH$_2$	31% @ 250 μM	-	>95
8a		H	Inactive @ 250 μM	-	>95
8b		H	24	0.33	>95
8c		NH$_2$	66	0.27	>95
8d		NH$_2$	74	0.28	>95
8e		NH$_2$	28	0.31	>95

^{a}See the Experimental Section for details.

were used: the Literature Substructures and Similarity Searching branches. As hypothesized, both branches successfully yielded inhibitors of BRD4(1). Overall, a hit rate of 2.5% was achieved for all of the compounds tested, and a hit rate of 4.2% was achieved for the 143 compounds selected by our virtual screening approach (Table 6). Strikingly, all of the active compounds had been identified from our virtual screen rather than from the control experiment, highlighting the success of the approach. We believe that the superiority of our virtual screening approach compared to the control branch is due to several factors. First of all, our KAc mimetic approach reduced the number of commercially available compounds sufficiently to enable docking, yet it ensured that a large number of KAc

mimetics were taken forward into the docking step. Second, the application of docking rather than just a similarity search ensured that the purchased compound have a high likelihood of meeting the tight geometric constraint of the KAc binding site. Finally, our extensive manual filtering and human input after docking removed several potential false positives.

Within the compounds selected by the virtual screen, 76 came from the Literature Substructures approach and two hits were identified. Sixty seven compounds came from the Similarity Searching approach, from which four of the six actives were identified. Four KAc mimetics that were unprecedented for bromodomain inhibition were discovered, fulfilling the main goal of this work.
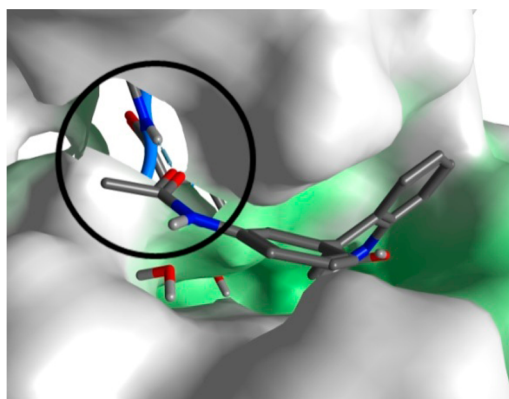
Figure 10. Interaction of the acetyl group of **5** with backbone donor of Asp88 in BRD4. Surface colors were generated using the pocket colors in MOE. Green represents an enclosed surface, and white, exposed. Alternate views of the binding mode of **5** can be seen in Figure 7D.
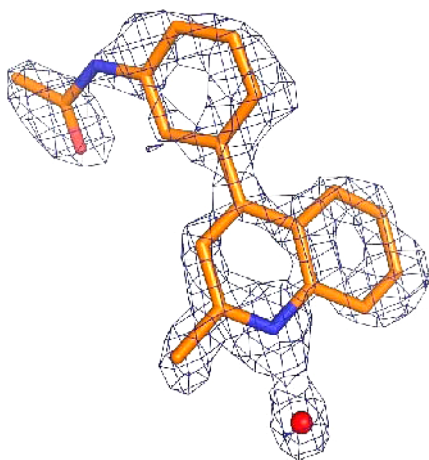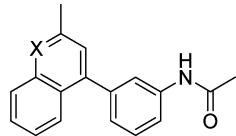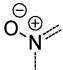

Figure 11. Electron density of **5** including a water molecule in close proximity to the quinoline nitrogen (2Fo−Fc map).

We initially expected that the Literature Substructures branch would yield the higher hit rate because of the presence of validated and structurally related warheads. Interestingly, this

Table 4. Activity of 5 and Its N-Oxide Derivative 14a

Compound number	X	IC$_{50}$^{a} (μM)	LE	UV Purity^a (%)
5	N	31% @ 250 μM	-	>95
14a	(N-oxide)	42	0.27	>95

^{a}See the Experimental Section for details.

turned out not to be the case, with a higher hit rate being achieved by the Similarity Searching branch. A possible reason for this observation is that the published inhibitors are optimized for the BRD4(1) binding site and possess good shape-complementarity as well as a KAc mimetic warhead. Compounds selected for the Literature Substructures branch possessed this warhead, but without optimization suboptimal binding in the upper part of the pocket may have abrogated any activity.

CONCLUSIONS
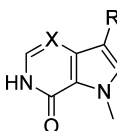
We describe a structure-based virtual screening approach to identify inhibitors of bromdomains together with the validation of this approach, resulting in the discovery of novel inhibitors of BRD4(1). The key elements of this approach are the extensive design and use of substructure queries to compile a set of commercially available compounds featuring novel putative KAc mimetics followed by subjection of this set to docking for final compound selection. Using this approach, we selected and tested 143 compounds and identified novel hits, including four unprecedented acetyl-lysine mimetics. A control experiment that failed to identify hits was also performed, further

Scheme 2. Synthetic Route to 5 and 14a^a
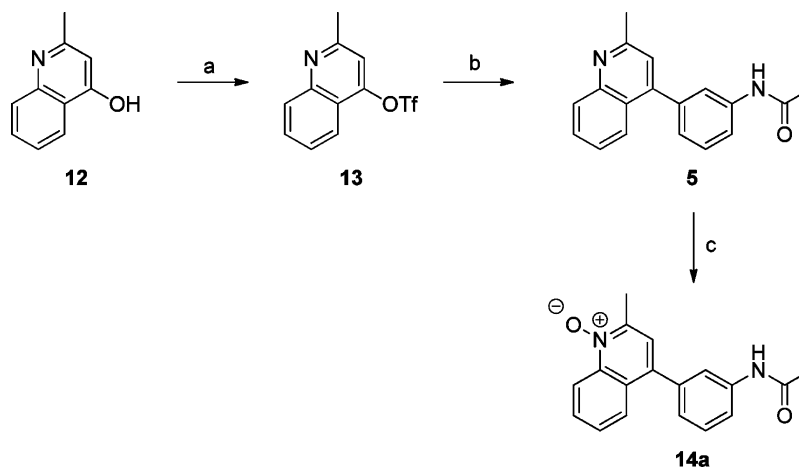
^{a}Reagents and conditions: (a) Tf$_2$O, Et$_3$N, CHCl$_3$, rt, 2 h; (b) acetamidophenylboronic acid, Pd(PPh$_3$)$_4$, CsCO$_3$, dioxane, 120 °C, 30 min; (c) mCPBA, DCM, reflux, 3 h.

Table 5. Activity of Derivatives of 6

15

Compound number	X	R	IC$_{50}$^{a} (μM)	LE	UV Purity^a (%)
6	CH	H	11% @ 100 μM	-	>95
15a	N	(p-tolyl)	31	0.34	94
15b	N	(4-fluorophenyl)	16	0.37	>95

^{a}See the Experimental Section for details.

Table 6. Summary of the Hit Rates for the 240 Compounds Screened against BRD4

approach	compounds tested	hits	hit rate (%)
all compounds	240	6	2.5
virtual screen	143	6	4.2
literature substructures	76	2	2.6
similarity searching	67	4	6.0
control set	97	0	0

confirming the success of our approach. The potency of many of the hits was initially modest. However, through use of cocrystal structures and structure-based design, we were able to improve the potency considerably into a range frequently found for screening hits. This work is therefore a good example of how novel but initially modestly potent compounds are identified with a fast and very limited screening effort and then quickly optimized through the use of cocrystal structures.

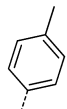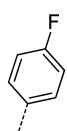Because of the similarity between bromodomain binding sites and the focus on the KAc mimetic, this approach is applicable to the large fraction of bromodomains for which structural information of sufficient resolution is available. Furthermore, we believe that the novel KAc mimetics disclosed here will serve as valuable starting points for the development of potent inhibitors of BRD4(1) and other related bromodomains.

■ **EXPERIMENTAL SECTION**

Computational Methods. *Ligands for Similarity Searches.* We used the ICR Vendor Collection, which is a library of 2.4 million commercially available compounds from 11 vendors for which details have been described by Langdon et al.[41]

Conformer and Protonation State Generation for Pharmacophore and Shape-Based Similarity Searching. Up to 100 conformations were generated using OMEGA.[42,43] Single protonation states were generated using FILTER.[44]

Choice of Template for Virtual Screen. At the time of performing the virtual screen against BRD4(1), the only inhibitors published were the triazolodiazepines, BIC1, and simple dihydroquinazolinones. A number of published structures were available, but the only suitable

ligand-bound structures were with triazolodiazepines. For this reason, the structure used for the virtual screen was that of (+)-JQ1 bound to the BRD4(1) (PDB ID: 3MXF), which was used in the structure-based pharmacophore searches and the bound pose of (+)-JQ1 for shape-based similarity searches, and it was also the structure used for the docking experiments. Water molecules with the following UIDs were treated as part of the pocket for docking experiments and pharmacophore excluded volumes: 9, 12, 15, 23, 33, and 209.

Pharmacophore Searches. We performed three pharmacophore searches on the basis of the (+)-JQ1 molecule bound to BRD4(1) (PDB ID: 3MXF) using the receptor as an excluded volume. The first pharmacophore was the most complex containing five points, including two acceptors from the triazole ring of (+)-JQ1, a hydrophobic substituent for the methyl group at the base of the pocket, and two further hydrophobic substituents at the ZA-channel and hydrophobic shelf positions of the binding site. This pharmacophore characterized each feature known to significantly contribute to the potency of (+)-JQ1 and found just 6540 matching ligands. The next pharmacophore was a derivative of the first, relaxing the requirement for both acceptors on the triazole ring to just one of the two. This increased the number of matching ligands significantly to 268 474. The third pharmacophore was also a derivative of the first one, but this time with the pharmacophoric point corresponding to the hydrophobic shelf removed. Again this increased the number of matching ligands but not as significantly as for the second pharmacophore to 41 890. The pharmacophore searches employed can be seen in Figure 12. All pharmacophore searches were performed using the Pharmacophore module in MOE.[45]
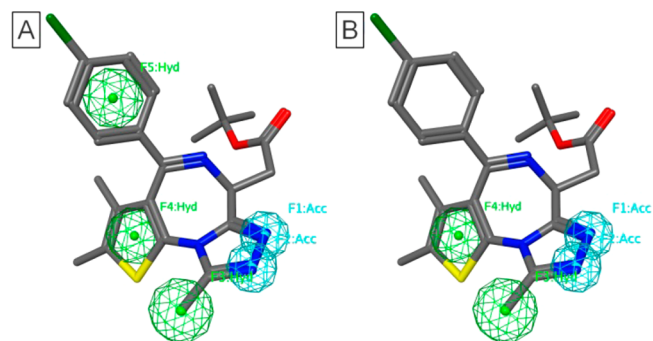
Figure 12. (A) Pharmacophore searches 1 and 2 (with 2 requiring only one acceptor). (B) Pharmacophore search 3.

Shape-Based Similarity Searches. We performed two shape-based similarity searches: one on the full (+)-JQ1 ligand in its bound conformation from PDB ID 3MXF and one on a reduced version of the ligand with the ester and chlorophenyl groups removed to focus on the KAc mimetic part of the binding site (Figure 13). Both searches were performed with two acceptor pharmacophore points from the triazole part of the (+)-JQ1 ligand. The top 100 000 compounds ranked by the TanimotoCombo scoring function from each search
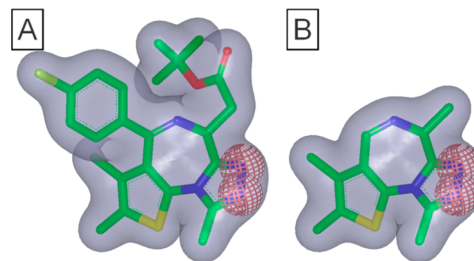
Figure 13. Shape-based similarity searches used with acceptor pharmacophoric points included (red spheres). (A) Full (+)-JQ1 ligand. (B) Reduced (+)-JQ1 ligand.

were taken through to subsequent docking steps. All shape-based similarity searches were performed in vROCS.[46,47]

Two-Dimensional Similarity Searches. A single 2D similarity search was performed using the ECFP4 fingerprint and the (+)-JQ1 ligand as a template in Pipeline Pilot.[48,49] The top 100 000 ligands ranked by Tanimoto similarity were taken through to subsequent docking steps.

Protein Preparation for Docking. Protons were added to PDB 3MXF using Protonate3D in MOE.[45] The structure was preprocessed using the protein preparation wizard[50] in Maestro,[51] with the assign bond orders, create disulfide bonds, and convert selenomethionines to methionines options selected. Grids for Glide docking were then generated using the receptor grid generation tool in Maestro using an enclosing box of size 20 Å around the center of (+)-JQ1 and other settings left at the default.

Ligand Preparation for Docking. Compounds were prepared using LigPrep[52] with default settings. Otherwise, Epik[53] was used for protonation-state assignment and tautomer generation.

Docking. Docking was performed using Glide with default settings.[54,55] For more than 5000 ligands, the compounds were initially docked using Glide in HTVS mode and the 5000 top ranked compounds by GlideScore were docked using Glide in SP mode. For fewer than 5000 ligands, the compounds were submitted directly to Glide in SP mode. Water molecules included were treated as rigid, with hydrogen positions used as defined by the Protonate3D step.

CSD Use. To analyze the observed dihedral angle of certain substructures in the CSD,[56] initial substructure searches and the dihedral in question were defined using Conquest and the data output and analyzed using Vista. A high-energy conformation was defined as one that possessed a dihedral angle not observed in the CSD for sufficiently populated substructures.

Biochemistry. *AlphaScreen.* Assays were performed as previously described.[40] All reagents were diluted in 50 mM HEPES, 100 mM NaCl, 0.1% BSA, pH 7.4 supplemented with 0.05% CHAPS and allowed to equilibrate to room temperature prior to addition to plates. A 24-point 1:2 serial dilution of the ligands was prepared over the range of 150−0 μM, and 4 μL was transferred to low-volume 384-well plates (ProxiPlateTM-384 Plus, PerkinElmer) followed by 4 μL of HIS-tagged protein (BRD4(1), 250 nM). The plates were sealed and incubated at room temperature for 30 min before the addition of 4 μL of biotinylated peptide at an equimolar concentration to the protein (the peptide used for BRD4(1): H-SGRGK(Ac)GGK(Ac)GLGK-(Ac)GGAK(Ac)RHRK(Biotin)-OH; Cambridge Research Biochemicals, UK). The plates were sealed and incubated for a further 30 min before the addition of 4 μL of streptavidin-coated donor beads (25 μg/mL) and 4 μL of nickel chelate acceptor beads (25 μg/mL) under low-light conditions. The plates were foil sealed to protect from light, incubated at room temperature for 60 min, and read on a PHERAstar FS plate reader (BMG Labtech) using an AlphaScreen 680 excitation/570 emission filter set. IC_{50} was calculated in Prism 5 (GraphPad Software) after normalization against corresponding DMSO controls, and they are given as the final concentration of compound in the 20 μL reaction volume.

Protein Expression and Purification. Proteins were cloned, expressed, and purified as previously described.[7]

Crystallization. Aliquots of the purified proteins were set up for crystallization using a mosquito crystallization robot (TTP Labtech). Coarse screens were typically set up onto Greiner 3-well plates using three different drop ratios of precipitant to protein per condition (100 + 50, 75 + 75, and 50 + 100 nL). Initial hits were optimized further by scaling up the drop sizes. All crystallizations were carried out using the sitting-drop vapor-diffusion method at 4 °C. BRD4(1) crystals with **1** were grown by mixing 150 nL of protein (9.9 mg/mL and 5 mM final ligand concentration) with an equal volume of reservoir solution containing 0.2 M sodium sulfate, 0.20 M NaBr, 0.1 M BTProp pH 8.5, 20.0% PEG6K, 10.0% ethylene glycol. BRD4(1) crystals with **3** were grown by mixing 100 nL of protein (9.0 mg/mL and 5 mM final ligand concentration) with 200 nL of reservoir solution containing 0.20 M Na(malonate), 0.1 M BTProp pH 8.5, 20.0% PEG3350, 10.0% ethylene glycol. BRD4(1) crystals with **4** were grown by mixing 150

nL of the protein (9.0 mg/mL and 10 mM final ligand concentration) with an equal volume of reservoir solution containing 0.20 M Na_2SO_4, 20.0% PEG3350 and 10.0% ethylene glycol. BRD4(1) crystals with **5** were grown by mixing 150 nL of protein (9.9 mg/mL and 5 mM final ligand concentration) with an equal volume of reservoir solution containing 0.2 M sodium sulfate, 0.20 M LiCl, 0.1 M Tris pH 8.0, 20.0% PEG6K, 10.0% ethylene glycol. In all cases, diffraction-quality crystals grew within a few days.

Data Collection and Structure solution. All crystals were cryo-protected using the well solution supplemented with additional ethylene glycol and were flash frozen in liquid nitrogen. Data were collected in-house on a Rigaku FRE rotating anode system equipped with a RAXIS-IV detector at 1.52 Å. Indexing and integration was carried out using MOSFLM,[57] and scaling was performed with SCALA.[58] Initial phases were calculated by molecular replacement with PHASER[59] using the known model of BRD4(1) (PDB ID: 2OSS). Initial models were built by ARP/wARP[60] followed by manual building in COOT.[61] Refinement was carried out in REFMAC5.[62] In all cases, thermal motions were analyzed using TLSMD,[63] and hydrogen atoms were included in late refinement cycles. Data collection and refinement statistics can be found in the Supporting Information, Table S1. The models and structure factors have been deposited with PDB accession codes 4MEP (BRD4(1)/ compound **1**), 4MEN (BRD4(1)/ compound **3**), 4MEQ (BRD4(1)/ compound **4**), and 4MEO (BRD4(1)/ compound **5**).

Chemistry. *General Experimental.* Commercially available starting materials, reagents, and dry solvents were used as supplied. Column chromatography was performed on a Biotage SP1 purification system using Biotage Flash silica cartridges. Reverse-phase chromatography was performed using isolute C18 silica columns. Semiprep HPLC purification was achieved using 1000 μL standard injections (with needle rinse) of the sample at a 20 mg/mL concentration in DMSO onto a Phenomenex Gemini column (10 μm, 250 × 21.2 mm, C18, Phenomenex). Chromatographic separation at room temperature was carried out using a Gilson GX-281 liquid handler system combined with a Gilson 322 HPLC pump (Gilson) over a 15 min gradient elution (Grad15 min20mlsLipo.m) from 40:60 to 100:0 methanol/water (both modified with 0.1% formic acid) at a flow rate of 20 mL/min. UV−vis spectra were acquired at 254 nm on a Gilson 156 UV−vis detector (Gilson). Collection was triggered by UV signal and collected using a Gilson GX-281 liquid handler system (Gilson). Raw data was processed using Gilson Trilution Software. LC−MS and HRMS analysis was performed on an Agilent 1200 series HPLC and diode array detector coupled to a 6210 time-of-flight mass spectrometer with dual multimode APCI/ESI source. Analytical separation was carried out at 30 °C on a Merck Purospher STAR column (RP-18e, 30 × 4 mm) using a flow rate of 1.5 mL/min in a 4 min gradient elution with detection at 254 nm. The mobile phase was a mixture of methanol (solvent A) and water containing formic acid at 0.1% (solvent B). Gradient elution was as follows: 1:9 (A/B) to 9:1 (A/B) over 2.5 min, 9:1 (A/B) for 1 min, and then reversion back to 1:9 (A/B) over 0.3 min, and finally 1:9 (A/B) for 0.2 min. ^{1}H NMR spectra were recorded on a Bruker Avance-500. Samples were prepared as solutions in a deuterated solvent and referenced to the appropriate internal nondeuterated solvent peak or tetramethylsilane. Purchased compounds were prepared from DMSO stocks with DMSO-d_6 added. Chemical shifts were recorded in ppm (δ) downfield of tetramethylsilane.

Compound 1. 3-Chloro-5-(1-(3-methylpyridin-2-yl)-3-phenyl-1*H*-1,2,4-triazol-5-yl)pyridin-2(1*H*)-one (**1**). Compound **1** was purchased as a 5 mg solid sample from ChemBridge (supplier ID 25722975). ^{1}H NMR (500 MHz, DMSO) δ 2.21 (s, 3H), 7.45 (s, 1H), 7.47−7.55 (m, 4H), 7.66 (t, 1H), 7.72 (s, 1H), 8.07 (d, 1H), 8.11 (d, 2H), 8.51 (d, 1H). HRMS m/z calcd for $C_{19}H_{15}ClN_5O$ [M + H]$^+$, 364.0960; found, 364.0961.

Compound 2. 3-Methyl-4-(3-(trifluoromethyl)phenyl)isoxazol-5-amine (**2**). Compound **2** was purchased as a 5 mg solid sample from Key Organics Ltd. (supplier ID 10T-0381). ^{1}H NMR (500 MHz, DMSO) δ 2.13 (s, 3H), 6.93 (s, 2H), 7.54−7.65 (m, 4H). HRMS m/z calcd for $C_{11}H_{10}F_3N_2O$ [M + H]$^+$, 243.0740; found, 243.0741.

Compound 3. *N*,5-Dimethyl-*N*-(4-methylbenzyl)-[1,2,4]triazolo-[1,5-*a*]pyrimidin-7-amine (**3**). Compound **3** was purchased as a 50 mg solid sample from Enamine Ltd. (supplier ID T6839820) and purified by semiprep HPLC. ^{1}H NMR (500 MHz, CDCl$_3$) δ 2.37 (s, 3H), 2.60 (s, 3H), 3.20 (s, 3H), 5.31 (s, 2H) 6.07 (s, 1H), 7.13–7.20 (m, 4H), 8.34 (s, 1H). HRMS *m/z* calcd for C$_{15}$H$_{18}$N$_5$ [M + H]$^+$, 268.1557; found, 268.1558.

Compound 4. 5-Methyl-7-phenyl-[1,2,4]triazolo[1,5-*a*]pyrimidin-2-amine (**4**). Compound **4** was purchased as a 5 mg solid sample from Princeton Biomolecular Research Inc. (supplier ID OSSK_397127). ^{1}H NMR (500 MHz, DMSO) δ 6.34 (s, 2H), 7.18 (s, 1H), 7.57–7.63 (m, 3H), 8.14 (d, 2H). The methyl peak was not observed and was expected to be below the DMSO peak. HRMS *m/z* calcd for C$_{12}$H$_{12}$N$_5$ [M + H]$^+$, 226.1087; found, 226.1091.

Compound 5. *N*-(3-(2-Methylquinolin-4-yl)phenyl)acetamide (**5**). Compound **5** was initially purchased as a 5 mg solid sample from ChemBridge (supplier ID 50866471). ^{1}H NMR (500 MHz, DMSO) δ 2.07 (s, 3H), 7.21 (d, 1H), 7.36 (s, 1H), 7.48–7.56 (m, 2H), 7.70 (d,1H), 7.75 (t, 1H), 7.81 (s, 1H), 7.84 (d, 1H), 8.01 (d, 1H), 10.14 (s, 1H). HRMS *m/z* calcd for C$_{18}$H$_{16}$N$_2$O [M + H]$^+$, 277.1335; found, 277.1333. Resynthesis of Compound **5**. 2-Methylquinolin-4-yl trifluoromethanesulfonate (**13**). Triflic anyhdride (0.95 mL, 5.65 mmol) was added to a solution of 2-methylquinolin-4-ol **12** (750 mg, 4.71 mmol) and triethylamine (0.66 mL, 4.71 mmol) in anhydrous DCM (5 mL) under nitrogen and stirred for 2 h. The reaction mixture was concentrated in vacuo. The resulting purple oil was purified by column chromatography (EtOAc to 5% MeOH in EtOAc) to afford title compound (863 mg, 63%). LC–MS (ESI, *m/z*) t_R 2.82 min, 292.18 [M + H]$^+$. ^{1}H NMR (500 MHz, CDCl$_3$) δ 2.87 (s, 3H), 7.35 (s, 1H), 7.68 (t, 1H), 7.86 (t, 1H), 8.05 (d, 1H), 8.17 (d, 1H).

N-(3-(2-Methylquinolin-4-yl)phenyl)acetamide (**5**). To a solution of 2-methylquinolin-4-yl trifluoromethanesulfonate **13** (280 mg, 0.79 mmol) in dioxane/water (2:1, 4.5 mL) were added acetamidophenylboronic acid (283 mg, 1.58 mmol), tetrakis triphenylphosphine palladium (45.6 mg, 0.04 mmol), and cesium carbonate (386 mg, 1.185 mmol). The reaction mixture was heated at 120 °C for 30 min under microwave conditions. The reaction mixture was diluted with EtOAc (20 mL) and washed with water (20 mL). The aqueous layer was re-extracted with EtOAc (20 mL), and the combined organic layers were dried (MgSO$_4$) and concentrated in vacuo. The residue was purified by column chromatography (20% EtOAc in hexane to 100% EtOAc) to afford the title compound (141 mg, 65%). LC–MS (ESI, *m/z*) t_R 1.97 min, 277.13 [M + H]$^+$. ^{1}H NMR (500 MHz, CDCl$_3$) δ 2.23 (s, 3H), 2.81 (s, 3H), 7.23–7.29 (m, 2H), 7.44–7.57 (m, 3H), 7.64–7.74 (m, 3H), 7.89 (d,1H), 8.15 (d, 1H). HRMS *m/z* calcd for C$_{18}$H$_{17}$N$_2$O [M + H]$^+$, 277.1335; found, 277.1336.

Compound 6. 1-Methyl-1*H*-pyrrolo[2,3-*c*]pyridin-7(6*H*)-one (**6**). Compound **6** was purchased as a 5 mg solid sample from Enamine Ltd. (supplier ID EN300−74511). ^{1}H NMR (500 MHz, DMSO) δ 4.05 (s, 3H), 6.24 (d, 1H), 6.39 (d, 1H), 6.81 (t, 1H), 7.26 (d, 1H), 10.81 (s, 1H). HRMS *m/z* calcd for C$_8$H$_9$N$_2$O [M + H]$^+$, 149.0709; found, 149.0709.

Compound 7a. 3-Chloro-5-(3-isopropyl-1-(3-methylpyridin-4-yl)-1*H*-1,2,4-triazol-5-yl)pyridin-2(1*H*)-one (**7a**). Compound **7a** was purchased as a 5 mg solid sample from ChemBridge (supplier ID 90638099). ^{1}H NMR (500 MHz, DMSO) δ 1.24 (m, 1H), 1.32 (d, 6H), 2.08 (s, 3H), 7.34 (s, 1H), 7.47 (d, 1H), 7.68 (s, 1H), 8.59 (d, 1H), 8.71 (s, 1H). HRMS *m/z* calcd for C$_{16}$H$_{17}$ClN$_5$O [M + H]$^+$, 330.1116; found, 330.1114.

Compound 7b. 3-Chloro-5-(1-(2,3-dihydrobenzo[*b*][1,4]dioxin-5-yl)-3-isobutyl-1*H*-1,2,4-triazol-5-yl)pyridin-2(1*H*)-one (**7b**). Compound **7b** was purchased as a 5 mg solid sample from ChemBridge (supplier ID 95921162). ^{1}H NMR (500 MHz, DMSO) δ 0.93−0.99 (m, 7H), 2.07 (s, 2H), 4.29 (s, 4H), 6.90 (d, 1H), 6.97−7.03 (m, 2H), 7.41 (s, 1H), 7.69 (s, 1H). HRMS *m/z* calcd for C$_{19}$H$_{20}$ClN$_4$O$_3$ [M + H]$^+$, 387.1218; found, 387.1207.

Compound 7c. 3-Chloro-5-(1-(4-fluorophenyl)-3-methyl-1*H*-1,2,4-triazol-5-yl)pyridin-2(1*H*)-one (**7c**). Compound **7c** was purchased as a 5 mg solid sample from ChemBridge (supplier ID 26575894). ^{1}H NMR (500 MHz, DMSO) δ 2.34 (s, 3H), 7.36−7.42 (m, 3H), 7.51–

7.57 (m, 2H), 7.66 (s, 1H). HRMS *m/z* calcd for C$_{14}$H$_{11}$ClFN$_4$O [M + H]$^+$, 305.0600; found, 305.0592.

Compound 8a. 5-Methyl-7-phenyl-[1,2,4]triazolo[1,5-*a*]pyrimidine (**8a**). Compound **8a** was purchased as a 5 mg solid sample from Enamine Ltd. (supplier ID T0510-0868). ^{1}H NMR (500 MHz, DMSO) δ 7.56 (s, 1H), 7.62−7.69 (m, 3H), 8.15−8.20 (m, 2H), 8.63 (s, 1H). The methyl peak was not observed and was expected to be below the DMSO peak. HRMS *m/z* calcd for C$_{12}$H$_{11}$N$_4$ [M + H]$^+$, 211.0978; found, 211.0976.

Compound 8b. *N*-((5-Chlorothiophen-2-yl)methyl)-*N*,5-dimethyl-[1,2,4]triazolo[1,5-*a*]pyrimidin-7-amine (**8b**). Compound **8b** was purchased as a 5 mg solid sample from Enamine Ltd. (supplier ID Z64611040). ^{1}H NMR (500 MHz, DMSO) δ 3.13 (s, 3H), 5.39 (s, 2H), 6.44 (s, 1H), 7.00 (s, 2H), 8.49 (s, 1H). The methyl peak was not observed and was expected to be below the DMSO peak. HRMS *m/z* calcd for C$_{12}$H$_{13}$ClN$_5$S [M + H]$^+$, 294.0575; found, 294.0571.

Synthesis of Compound 8c. 7-Chloro-5-methyl-[1,2,4]triazolo[1,5-*a*]pyrimidin-2-amine (**10**). 2-Amino-5-methyl-[1,2,4]triazolo[1,5-*a*]-pyrimidin-7(3*H*)-one **9** (500 mg, 3.028 mmol) was added to cooled (0 °C), stirring POCl$_3$ (3 mL). The reaction mixture was allowed to warm to rt and was heated to reflux for 2 h. The reaction mixture was concentrated in vacuo, and the residue was dissolved in DCM (20 mL). Water (20 mL) was added, and the resultant precipitate was isolated by filtration. The residue was purified by triturating with DCM and used in subsequent reactions without further purification (345 mg, 62%). LC−MS (ESI, *m/z*) t_R 1.15 min, did not ionize [M + H]$^+$. ^{1}H NMR (500 MHz, TFA) δ 2.91 (s, 3H), 7.72 (s, 1H).

N-Methyl-1-(p-tolyl)methanamine. 4-Methylbenzyl chloride (0.933 mL, 7.112 mmol) was added to a solution of 40% aqueous methylamine (10 mL, 18.031 mmol) in EtOH (10 mL) and stirred at rt for 12 h. The reaction mixture was concentrated in vacuo, the residue was dissolved in water (20 mL), and the pH adjusted to 12 with 2 M NaOH. The aqueous layer was extracted with EtOAc (2 × 20 mL). The combined organic layers were dried (MgSO$_4$) and concentrated in vacuo. The resulting yellow oil was purified by reverse-phase C18 flash column chromatography (water) to afford the title compound (112 mg, 12%). LC−MS (ESI, *m/z*) t_R 0.85 min, 136.11 [M + H]$^+$. ^{1}H NMR (500 MHz, CDCl$_3$) δ 2.36 (s, 3H), 2.46 (s, 3H), 3.73 (s, 2H), 7.15 (d, 2H), 7.22 (d, 2H).

N^7,5-Dimethyl-*N*^{7}-(4-methylbenzyl)-[1,2,4]triazolo[1,5-*a*]-pyrimidine-2,7-diamine (**8c**). 7-Chloro-5-methyl-[1,2,4]triazolo[1,5-*a*]pyrimidin-2-amine **10** (50 mg, 0.275 mmol) was added to a stirred solution of *N*-methyl-1-(p-tolyl)methanamine (74 mg, 0.55 mmol) and K$_2$CO$_3$ (38 mg, 0.275 mmol) in anhydrous ethanol (0.5 mL). The reaction mixture was heated to reflux for 2 h. The reaction mixture was concentrated in vacuo, and the residue was dissolved in EtOAc (10 mL) and water (10 mL). The aqueous layer was re-extracted with EtOAc (10 mL), and the combined organic layers were dried (MgSO$_4$) and concentrated in vacuo. The residue was purified using an SCX-2 column (MeOH) to afford the title compound (5.63 mg, 42%). LC−MS (ESI, *m/z*) t_R 2.63 min, 283.17 [M + H]$^+$. ^{1}H NMR (500 MHz, CDCl$_3$) δ 2.36 (s, 3H), 2.49 (s, 3H), 3.08 (s, 3H), 4.66 (brs, 2H), 5.19 (s, 2H), 5.94 (s, 1H), 7.12 (d, 2H), 7.15 (d, 2H). HRMS *m/z* calcd for C$_{15}$H$_{19}$N$_6$ [M + H]$^+$, 283.1666; found, 283.1665.

Compound 8d. 5-Methyl-*N*^{7}-(4-methylbenzyl)-[1,2,4]triazolo[1,5-*a*]pyrimidine-2,7-diamine (**8d**). 7-Chloro-5-methyl-[1,2,4]triazolo[1,5-*a*]pyrimidin-2-amine **10** (50 mg, 0.275 mmol) was added to a stirred solution of *p*-tolylmethanamine (1.36 mmol) and K$_2$CO$_3$ (38 mg, 0.275 mmol) in anhydrous ethanol (0.5 mL). The reaction mixture was heated to reflux for 2 h, with reaction progress monitored by LC−MS. The reaction mixture was concentrated in vacuo. The residue was dissolved in ethyl acetate (10 mL) and water (10 mL). The aqueous layer was re-extracted with ethyl acetate, and the combined organic layers were dried (MgSO$_4$) and concentrated in vacuo. The residue was purified by column chromatography (0% MeOH in EtOAc to 20% MeOH in EtOAc) to afford the title compound (31 mg, 42%). LC−MS (ESI, *m/z*) t_R 2.47 min, 269.15 [M + H]$^+$. ^{1}H NMR (500 MHz, CDCl$_3$) δ 2.38 (s, 3H), 2.48 (s, 3H), 4.51 (d, 2H), 4.61 (brs, 2H) 5.94 (s, 1H), 6.14 (s, 1H), 7.21 (d, 2H), 7.24 (d, 2H). HRMS *m/z* calcd for C$_{14}$H$_{17}$N$_6$ [M + H]$^+$, 269.1509; found, 269.1510.

Compound 8e. N^7-((5-Chlorothiophen-2-yl)methyl)-N^7,5-dimeth-yl-[1,2,4]triazolo[1,5-*a*]pyrimidine-2,7-diamine (**8e**). 7-Chloro-5-methyl-[1,2,4]triazolo[1,5-*a*]pyrimidin-2-amine **10** (50 mg, 0.275 mmol) was added to a stirred solution of 1-(5-chlorothiophen-2-yl)-*N*-methylmethanamine (111 mg, 0.688 mmol) and K$_2$CO$_3$ (38 mg, 0.275 mmol) in anhydrous ethanol (0.5 mL). The reaction mixture was heated to reflux for 2 h, with reaction progress monitored by LC−MS. The reaction mixture was concentrated in vacuo. The residue was dissolved in ethyl acetate (10 mL) and water (10 mL). The aqueous layer was re-extracted with ethyl acetate, and the combined organic layers were dried (MgSO$_4$) and concentrated in vacuo The residue was purified by column chromatography (0% MeOH in DCM to 10% MeOH in DCM) to afford the title compound (4.32 mg, 42%). LC−MS (ESI, *m/z*) t_R 2.71 min, 309.07 [M + H]$^+$. ^{1}H NMR (500 MHz, CDCl$_3$) δ 2.50 (s, 3H), 3.07 (s, 3H), 4.75 (brs, 2H), 5.29 (s, 2H), 5.95 (s, 1H), 6.77 (m, 2H). HRMS *m/z* calcd for C$_{12}$H$_{14}$ClN$_6$S [M + H]$^+$, 309.0684; found, 309.0684.

Compound 14a. 4-(3-Acetamidophenyl)-2-methylquinoline 1-oxide (**14a**). mCPBA (37.5 mg, 0.317 mmol) was added slowly to a stirring solution of *N*-(3-(2-methylquinolin-4-yl)phenyl)acetamide **5** (50 mg, 0.181 mmol) in anhydrous DCM (1.3 mL). The reaction mixture was heated at 45 °C for 3 h. The reaction mixture was cooled to room temperature and quenched with aq sat. sodium thiosulfate solution (1.5 mL) and aq sat. sodium bicarbonate solution (4.5 mL). The reaction mixture was extracted with DCM (2 × 10 mL), dried (MgSO$_4$), and concentrated in vacuo. The residue was purified by column chromatography (0% MeOH in DCM to 10% MeOH in DCM) to afford the title compound (7.2 mg, 14%). LC−MS (ESI, *m/z*) t_R 2.61 min, 293.13 [M + H]$^+$. ^{1}H NMR (500 MHz, CDCl$_3$) δ 2.17 (s, 3H), 3.04 (s, 3H), 7.19 (d, 1H), 7.28 (s, 1H), 7.46 (t, 1H), 7.60−7.66 (m, 2H), 7.69 (d, 1H), 7.86 (t, 1H), 7.97 (d, 1H), 8.10 (brs, 1H), 8.82 (d, 1H). HRMS *m/z* calcd for C$_{18}$H$_{17}$N$_2$O$_2$ [M + H]$^+$, 293.1285; found, 293.1287.

Compound 15a. 5-Methyl-7-(*p*-tolyl)-3*H*-pyrrolo[3,2-*d*]pyrimidin-4(5*H*)-one (**15a**). Compound **15a** was purchased as a 5 mg solid sample from Sigma-Aldrich (supplier CNC ID 310754082). ^{1}H NMR (500 MHz, DMSO) δ 2.30 (s, 3H), 4.03 (s, 3H), 7.18 (d, 2H), 7.80 (d, 1H), 7.85 (s, 1H), 7.89 (d, 2H), 12.15 (s, 1H). HRMS *m/z* calcd for C$_{14}$H$_{13}$N$_3$O [M + H]$^+$, 240.1131; found, 240.1133.

Compound 15b. 7-(4-Fluorophenyl)-5-methyl-3*H*-pyrrolo[3,2-*d*]-pyrimidin-4(5*H*)-one (**15b**). Compound **15b** was purchased as a 5 mg solid sample from Sigma-Aldrich (supplier CNC ID 310754657). ^{1}H NMR (500 MHz, DMSO) δ 4.08 (s, 3H), 7.22 (t, 2H), 7.87 (1H, s), 7.88 (1H, s), 8.06 (2H, dd), 12.03 (1H, s). HRMS *m/z* calcd for C$_{13}$H$_{11}$FN$_3$O [M + H]$^+$, 244.0881; found, 244.0877.

ASSOCIATED CONTENT

Ⓢ Supporting Information

Substructures used in the "Literature Substructures" approach, docking poses used to select active compounds, triazolopyr-imidine compounds purchased, and protein crystallography data collection and statistics. This material is available free of charge via the Internet at http://pubs.acs.org.

AUTHOR INFORMATION

Corresponding Authors

*Phone: +44 1865617584; E-mail: stefan.knapp@sgc.ox.ac.uk (S.K.).
*Phone: +44 2087224353; E-mail: swen.hoelder@icr.ac.uk (S.H.).

Notes

The authors declare no competing financial interest.

ABBREVIATIONS USED

2D, two dimensional; 3D, three dimensional; ATAD, AAA domain-containing protein; BET, bromodomain and extra terminal; BRD, bromodomain-containing protein; brs, broad singlet; CSD, Cambridge Structural Database; dd, doublet of doublets; ECFP, extended connectivity fingerprint; Glide, grid-based ligand docking with energetics; HA, heavy atom; HTVS, high-throughput virtual screening; KAc, acetyl-lysine; LE, ligand efficiency; MOE, molecular operating environment; ROCS, rapid overlay of chemical structures; SP, standard precision; VS, virtual screen

REFERENCES

(1) Muller, S.; Filippakopoulos, P.; Knapp, S. Bromodomains as therapeutic targets. *Expert Rev. Mol. Med.* **2011**, *13*, e29-1−e29-21.

(2) Filippakopoulos, P.; Picaud, S.; Mangos, M..; Keates, T.; Lambert, J.-P.; Barsyte-Lovejoy, D.; Felletar, I.; Volkmer, R.; Müller, S.; Pawson, T.; Gingras, A.-C.; Arrowsmith, C. H.; Knapp, S. Histone recognition and large-scale structural analysis of the human bromodomain family. *Cell* **2012**, *149*, 214−231.

(3) Vidler, L. R.; Brown, N.; Knapp, S.; Hoelder, S. Druggability analysis and structural classification of bromodomain acetyl-lysine binding sites. *J. Med. Chem.* **2012**, *55*, 7346−7359.

(4) Zeng, L.; Zhou, M.-M. Bromodomain: An acetyl-lysine binding domain. *FEBS Lett.* **2002**, *513*, 124−128.

(5) Mujtaba, S.; Zeng, L.; Zhou, M.-M. Structure and acetyl-lysine recognition of the bromodomain. *Oncogene* **2007**, *26*, 5521−5527.

(6) Filippakopoulos, P.; Knapp, S. The bromodomain interaction module. *FEBS Lett.* **2012**, *586*, 2692−2704.

(7) Filippakopoulos, P.; Qi, J.; Picaud, S.; Shen, Y.; Smith, W. B.; Fedorov, O.; Morse, E. M.; Keates, T.; Hickman, T. T.; Felletar, I.; Philpott, M.; Munro, S.; McKeown, M. R.; Wang, Y.; Christie, A. L.; West, N.; Cameron, M. J.; Schwartz, B.; Heightman, T. D.; Thangue, N. L.; French, C. A.; Wiest, O.; Kung, A. L.; Knapp, S.; Bradner, J. E. Selective inhibition of BET bromodomains. *Nature* **2010**, *468*, 1067−1073.

(8) Chung, C.; Coste, H.; White, J. H.; Mirguet, O.; Wilde, J.; Gosmini, R. L.; Delves, C.; Magny, S. M.; Woodward, R.; Hughes, S. A.; Boursier, E. V.; Flynn, H.; Bouillot, A. M.; Bamborough, P.; Brusq, J.-M. G.; Gellibert, F. J.; Jones, E. J.; Riou, A. M.; Homes, P.; Martin, S. L.; Uings, I. J.; Toum, J.; Clément, C. A.; Boullay, A.-B.; Grimley, R. L.; Blandel, F. M.; Prinjha, R. K.; Lee, K.; Kirilovsky, J.; Nicodeme, E. Discovery and characterization of small molecule inhibitors of the BET family bromodomains. *J. Med. Chem.* **2011**, *54*, 3827−3838.

(9) Seal, J.; Lamotte, Y.; Donche, F.; Bouillot, A.; Mirguet, O.; Gellibert, F.; Nicodeme, E.; Krysa, G.; Kirilovsky, J.; Beinke, S.; McCleary, S.; Rioja, I.; Bamborough, P.; Chung, C.-W.; Gordon, L.; Lewis, T.; Walker, A. L.; Cutler, L.; Lugo, D.; Wilson, D. M.; Witherington, J.; Lee, K.; Prinjha, R. K. Identification of a novel series of BET family bromodomain inhibitors: Binding mode and profile of I-BET151 (GSK1210151A). *Bioorg. Med. Chem. Lett.* **2012**, *22*, 2968−2972.

(10) Mirguet, O.; Lamotte, Y.; Donche, F.; Toum, J.; Gellibert, F.; Bouillot, A.; Gosmini, R.; Nguyen, V.-L.; Delannée, D.; Seal, J.; Blandel, F.; Boullay, A.-B.; Boursier, E.; Martin, S.; Brusq, J.-M.; Krysa, G.; Riou, A.; Tellier, R.; Costaz, A.; Huet, P.; Dudit, Y.; Trottet, L.; Kirilovsky, J.; Nicodeme, E. From ApoA1 upregulation to BET family bromodomain inhibition: Discovery of I-BET151. *Bioorg. Med. Chem. Lett.* **2012**, *22*, 2963−2967.

(11) Fish, P. V.; Filippakopoulos, P.; Bish, G.; Brennan, P. E.; Bunnage, M. E.; Cook, A. S.; Federov, O.; Gerstenberger, B. S.; Jones, H.; Knapp, S.; Marsden, B.; Nocka, K.; Owen, D. R.; Philpott, M.; Picaud, S.; Primiano, M. J.; Ralph, M. J.; Sciammetta, N.; Trzupek, J. D. Identification of a chemical probe for bromo and extra C-terminal bromodomain inhibition through optimization of a fragment-derived hit. *J. Med. Chem.* **2012**, *55*, 9831−9837.

(12) Nicodeme, E.; Jeffrey, K. L.; Schaefer, U.; Beinke, S.; Dewell, S.; Chung, C.; Chandwani, R.; Marazzi, I.; Wilson, P.; Coste, H.; White, J.; Kirilovsky, J.; Rice, C. M.; Lora, J. M.; Prinjha, R. K.; Lee, K.; Tarakhovsky, A. Suppression of inflammation by a synthetic histone mimic. *Nature* **2010**, *468*, 1119−1123.

(13) Belkina, A. C.; Denis, G. V. BET domain co-regulators in obesity, inflammation and cancer. *Nat. Rev. Cancer* **2012**, *12*, 465−477.

(14) Zuber, J.; Shi, J.; Wang, E.; Rappaport, A. R.; Herrmann, H.; Sison, E. A.; Magoon, D.; Qi, J.; Blatt, K.; Wunderlich, M.; Taylor, M. J.; Johns, C.; Chicas, A.; Mulloy, J. C.; Kogan, S. C.; Brown, P.; Valent, P.; Bradner, J. E.; Lowe, S. W.; Vakoc, C. R. RNAi screen identifies Brd4 as a therapeutic target in acute myeloid leukaemia. *Nature* **2011**, *478*, 524−528.

(15) Blobel, G. A.; Kalota, A.; Sanchez, P. V.; Carroll, M. Short hairpin RNA screen reveals bromodomain proteins as novel targets in acute myeloid leukemia. *Cancer Cell* **2011**, *20*, 287−288.

(16) Lockwood, W. W.; Zejnullahu, K.; Bradner, J. E.; Varmus, H. Sensitivity of human lung adenocarcinoma cell lines to targeted inhibition of BET epigenetic signaling proteins. *Proc. Natl. Acad. Sci. U.S.A.* **2012**, *109*, 19408−19413.

(17) Cheng, Z.; Gong, Y.; Ma, Y.; Lu, K.; Lu, X.; Pierce, L. A.; Thompson, R. C.; Muller, S.; Knapp, S.; Wang, J. Inhibition of BET bromodomain targets genetically diverse glioblastoma. *Clin. Cancer Res.* **2013**, *19*, 1748−1759.

(18) Puissant, A.; Frumm, S. M.; Alexe, G.; Bassil, C. F.; Qi, J.; Chanthery, Y. H.; Nekritz, E. A.; Zeid, R.; Gustafson, W. C.; Greninger, P.; Garnett, M. J.; McDermott, U.; Benes, C. H.; Kung, A. L.; Weiss, W. A.; Bradner, J. E.; Stegmaier, K. Targeting MYCN in neuroblastoma by BET bromodomain inhibition. *Cancer Discovery* **2013**, *3*, 308−323.

(19) Furdas, S. D.; Carlino, L.; Sippl, W.; Jung, M. Inhibition of bromodomain-mediated protein−protein interactions as a novel therapeutic strategy. *MedChemComm* **2012**, *3*, 123−134.

(20) Filippakopoulos, P.; Picaud, S.; Fedorov, O.; Keller, M.; Wrobel, M.; Morgenstern, O.; Bracher, F.; Knapp, S. Benzodiazepines and benzotriazepines as protein interaction inhibitors targeting bromodomains of the BET family. *Bioorg. Med. Chem.* **2012**, *20*, 1878−1886.

(21) Hewings, D. S.; Wang, M.; Philpott, M.; Fedorov, O.; Uttarkar, S.; Filippakopoulos, P.; Picaud, S.; Vuppusetty, C.; Marsden, B.; Knapp, S.; Conway, S. J.; Heightman, T. D. 3,5-Dimethylisoxazoles act as acetyl-lysine-mimetic bromodomain ligands. *J. Med. Chem.* **2011**, *54*, 6761−6770.

(22) Hewings, D. S.; Fedorov, O.; Filippakopoulos, P.; Martin, S.; Picaud, S.; Tumber, A.; Wells, C.; Olcina, M. M.; Freeman, K.; Gill, A.; Ritchie, A. J.; Sheppard, D. W.; Russell, A. J.; Hammond, E. M.; Knapp, S.; Brennan, P. E.; Conway, S. J. Optimization of 3,5-dimethylisoxazole derivatives as potent bromodomain ligands. *J. Med. Chem.* **2013**, *56*, 3217−3227.

(23) Hay, D.; Fedorov, O.; Filippakopoulos, P.; Martin, S.; Philpott, M.; Picaud, S.; Hewings, D. S.; Uttarkar, S.; Heightman, T. D.; Conway, S. J. The design and synthesis of 5-and 6-isoxazolylbenzimidazoles as selective inhibitors of the BET bromodomains. *MedChemComm* **2013**, *4*, 140−144.

(24) Dawson, M. A.; Prinjha, R. K.; Dittmann, A.; Giotopoulos, G.; Bantscheff, M.; Chan, W.; Robson, S. C.; Chung, C.; Hopf, C.;

Savitski, M. M.; Huthmacher, C.; Gudgin, E.; Lugo, D.; Beinke, S.; Chapman, T. D.; Roberts, E. J.; Soden, P. E.; Auger, K. R.; Mirguet, O.; Doehner, K.; Delwel, R.; Burnett, A. K.; Jeffrey, P.; Drewes, G.; Lee, K.; Huntly, B. J. P.; Kouzarides, T. Inhibition of BET recruitment to chromatin as an effective treatment for MLL-fusion leukaemia. *Nature* **2011**, *478*, 529−533.

(25) Bamborough, P.; Diallo, H.; Goodacre, J. D.; Gordon, L.; Lewis, A.; Seal, J. T.; Wilson, D. M.; Woodrow, M. D.; Chung, C. Fragment-based discovery of bromodomain inhibitors part 2: Optimization of phenylisoxazole sulfonamides. *J. Med. Chem.* **2011**, *55*, 587−596.

(26) Chung, C.; Dean, A. W.; Woolven, J. M.; Bamborough, P. Fragment-based discovery of bromodomain inhibitors part 1: Inhibitor binding modes and implications for lead discovery. *J. Med. Chem.* **2011**, *55*, 576−586.

(27) Picaud, S.; Costa, D. D.; Thanasopoulou, A.; Filippakopoulos, P.; Fish, P. V.; Philpott, M.; Fedorov, O.; Brennan, P.; Bunnage, M. E.; Owen, D. R.; Bradner, J. E.; Taniere, P.; O'Sullivan, B.; Müller, S.; Schwaller, J.; Stankovic, T.; Knapp, S. PFI-1, a highly selective protein interaction inhibitor, targeting BET bromodomains. *Cancer Res.* **2013**, *73*, 3336−3346.

(28) Ito, A.; Yokoyama, S.; Padmanabhan, B.; Shirouzu, M.; Terada, T.; Nishino, N.; Nakamura, Y.; Sasaki, K.; Umehara, T.; Ito, T.; Yoshida, M. Real-time imaging of histone H4K12-specific acetylation determines the modes of action of histone deacetylase and bromodomain inhibitors. *Chem. Biol.* **2011**, *18*, 495−507.

(29) Zhao, L.; Cao, D.; Chen, T.; Wang, Y.; Miao, Z.-H.; Xu, Y.; Chen, W.; Wang, X.; Li, Y.; Du, Z.; Xiong, B.; Li, J.; Xu, C.; Zhang, N.; He, J.; Shen, J. Fragment-based drug discovery of 2-thiazolidinones as inhibitors of the histone reader BRD4 bromodomain. *J. Med. Chem.* **2013**, *56*, 3833−3851.

(30) eMolecules Home Page. http://www.emolecules.com/.

(31) Bissantz, C.; Folkers, G.; Rognan, D. Protein-based virtual screening of chemical databases. 1. Evaluation of different docking/scoring combinations. *J. Med. Chem.* **2000**, *43*, 4759−4767.

(32) Warren, G. L.; Andrews, C. W.; Capelli, A.-M.; Clarke, B.; LaLonde, J.; Lambert, M. H.; Lindvall, M.; Nevins, N.; Semus, S. F.; Senger, S.; Tedesco, G.; Wall, I. D.; Woolven, J. M.; Peishoff, C. E.; Head, M. S. A critical assessment of docking programs and scoring functions. *J. Med. Chem.* **2005**, *49*, 5912−5931.

(33) Leach, A. R.; Shoichet, B. K.; Peishoff, C. E. Prediction of protein−ligand interactions. Docking and scoring: Successes and gaps. *J. Med. Chem.* **2006**, *49*, 5851−5855.

(34) Repasky, M.; Murphy, R.; Banks, J.; Greenwood, J.; Tubert-Brohman, I.; Bhat, S.; Friesner, R. Docking performance of the glide program as evaluated on the Astex and DUD datasets: A complete set of glide SP results and selected results for a new scoring function integrating WaterMap and glide. *J. Comput.-Aided Mol. Des.* **2012**, *26*, 787−799.

(35) Ferreira, R. S.; Simeonov, A.; Jadhav, A.; Eidam, O.; Mott, B. T.; Keiser, M. J.; McKerrow, J. H.; Maloney, D. J.; Irwin, J. J.; Shoichet, B. K. Complementarity between a docking and a high-throughput screen in discovering new cruzain inhibitors. *J. Med. Chem.* **2010**, *53*, 4891−4905.

(36) Baell, J. B.; Holloway, G. A. New substructure filters for removal of pan assay interference compounds (PAINS) from screening libraries and for their exclusion in bioassays. *J. Med. Chem.* **2010**, *53*, 2719−2740.

(37) McGaughey, G. B.; Sheridan, R. P.; Bayly, C. I.; Culberson, J. C.; Kreatsoulas, C.; Lindsley, S.; Maiorov, V.; Truchon, J.-F.; Cornell, W. D. Comparison of topological, shape, and docking methods in virtual screening. *J. Chem. Inf. Model.* **2007**, *47*, 1504−1519.

(38) Evers, A.; Hessler, G.; Matter, H.; Klabunde, T. Virtual screening of biogenic amine-binding g-protein coupled receptors: Comparative evaluation of protein- and ligand-based virtual screening protocols. *J. Med. Chem.* **2005**, *48*, 5448−5465.

(39) Bemis, G. W.; Murcko, M. A. The properties of known drugs. 1. Molecular frameworks. *J. Med. Chem.* **1996**, *39*, 2887−2893.

(40) Philpott, M.; Yang, J.; Tumber, T.; Fedorov, O.; Uttarkar, S.; Filippakopoulos, P.; Picaud, S.; Keates, T.; Felletar, I.; Ciulli, A.;

Knapp, S.; Heightman, T. D. Bromodomain-peptide displacement assays for interactome mapping and inhibitor discovery. *Mol. BioSyst.* **2011**, *7*, 2899−2908.

(41) Langdon, S. R.; Westwood, I. M.; Van Montfort, R. L. M.; Brown, N.; Blagg, J. Scaffold-focused virtual screening: Prospective application to the discovery of TTK inhibitors. *J. Chem. Inf. Model.* **2013**, *53*, 1100−1112.

(42) Hawkins, P. C. D.; Skillman, A. G.; Warren, G. L.; Ellingson, B. A.; Stahl, M. T. Conformer generation with OMEGA: Algorithm and validation using high quality structures from the Protein Databank and Cambridge Structural Database. *J. Chem. Inf. Model.* **2010**, *50*, 572−284.

(43) *OMEGA*; OpenEye Scientific Software: Santa Fe, NM; http://www.eyesopen.com/.

(44) *FILTER*; OpenEye Scientific Software: Santa Fe, NM; http://www.eyesopen.com/.

(45) *MOE*; Chemical Computing Group: Montreal, Quebec, Canada; http://www.chemcomp.com/.

(46) Grant, J. A.; Gallardo, M. A.; Pickup, B. T. A fast method of molecular shape comparison: A simple application of a Gaussian description of molecular shape. *J. Comput. Chem.* **1996**, *17*, 1653−1666.

(47) *vROCS*; OpenEye Scientific Software: Santa Fe, NM; http://www.eyesopen.com/.

(48) Bender, A.; Jenkins, J. L.; Scheiber, J.; Sukuru, S. C. K.; Glick, M.; Davies, J. W. How similar are similarity searching methods? A principal component analysis of molecular descriptor space. *J. Chem. Inf. Model.* **2009**, *49*, 108−119.

(49) *Pipeline Pilot*; Accelrys, Inc.: San Diego, CA; http://www.accelrys.com/.

(50) *Protein Preparation Wizard*; Schrödinger, LLC: Portland, OR; http://www.schrodinger.com/.

(51) *Maestro*; Schrödinger, LLC: Portland, OR; http://www.schrodinger.com/.

(52) *LigPrep*; Schrödinger, LLC: Portland, OR; http://www.schrodinger.com/.

(53) *Epik*; Schrödinger, LLC: Portland, OR; http://www.schrodinger.com/.

(54) *Glide*; Schrödinger, LLC: Portland, OR; http://www.schrodinger.com/.

(55) Friesner, R. A.; Banks, J. L.; Murphy, R. B.; Halgren, T. A.; Klicic, J. J.; Mainz, D. T.; Repasky, M. P.; Knoll, E. H.; Shaw, D. E.; Shelley, M.; Perry, J. K.; Francis, P.; Shenkin, P. S. Glide: A new approach for rapid, accurate docking and scoring. 1. Method and assessment of docking accuracy. *J. Med. Chem.* **2004**, *47*, 1739−1749.

(56) *CSD System*; CCDC: Cambridge, United Kingdom; http://www.ccdc.cam.ac.uk/.

(57) Leslie, A. G. W.; Powell, H. *MOSFLM 7.01*; MRC Laboratory of Molecular Biology: Cambridge, United Kingdom.

(58) Evans, P. *SCALA - Scale Together Multiple Observations of Reflections*, version 3.3.0; MRC Laboratory of Molecular Biology: Cambridge, United Kingdom.

(59) McCoy, A. J.; Grosse-Kunstleve, R. W.; Storoni, L. C.; Read, R. J. Likelihood-enhanced fast translation functions. *Acta Crystallogr., Sect. D* **2005**, *61*, 458−464.

(60) Perrakis, A.; Morris, R.; Lamzin, V. S. Automated protein model building combined with iterative structure refinement. *Nat. Struct. Mol. Biol.* **1999**, *6*, 458−463.

(61) Emsley, P.; Cowtan, K. Coot: Model-building tools for molecular graphics. *Acta Crystallogr., Sect. D* **2004**, *60*, 2126−2132.

(62) Murshudov, G. N.; Vagin, A. A.; Dodson, E. J. Refinement of macromolecular structures by the maximum-likelihood method. *Acta Crystallogr., Sect. D* **1997**, *53*, 240−255.

(63) Painter, J.; Merritt, E. A. Optimal description of a protein structure in terms of multiple groups undergoing TLS motion. *Acta Crystallogr., Sect. D* **2006**, *62*, 439−450.